ER sliding dynamics and ER–mitochondrial contacts occur on acetylated microtubules

Jonathan R. Friedman,[2] Brant M. Webster,[2] David N. Mastronarde,[1,2] Kristen J. Verhey,[3] and Gia K. Voeltz[2]

[1]Boulder Laboratory for Three-Dimensional Electron Microscopy of Cells, [2]Department of Molecular, Cellular, and Developmental Biology, University of Colorado at Boulder, Boulder, CO 80309
[3]Department of Cell and Developmental Biology, University of Michigan, Ann Arbor, MI 48109

The endoplasmic reticulum (ER) network is extremely dynamic in animal cells, yet little is known about the mechanism and function of its movements. The most common ER dynamic, termed ER sliding, involves ER tubule extension along stable microtubules (MTs). In this study, we show that ER sliding occurs on nocodazole-resistant MTs that are posttranslationally modified by acetylation. We demonstrate that high MT curvature is a good indicator of MT acetylation and show in live cells that ER sliding occurs predominantly on these curved, acetylated MTs. Furthermore, increasing MT acetylation by drug treatment increases the frequency of ER sliding. One purpose of the ER sliding on modified MT tracts could be to regulate its interorganelle contacts. We find that all mitochondria and many endosomes maintain contact with the ER despite the movements of each. However, mitochondria, but not endosomes, preferentially localize to acetylated MTs. Thus, different ER dynamics may occur on distinct MT populations to establish or maintain contacts with different organelles.

Introduction

The ER is a large organelle that spreads throughout the cytoplasm as a continuous network of tubules and sheets with a single lumen (Baumann and Walz, 2001; English et al., 2009). The interconnected ER network is constantly reorganizing its structure as new ER tubules grow out of existing ones, old tubules retract, sheets move, and new junctions are formed by fusion between ER membranes (Lee and Chen, 1988; Waterman-Storer and Salmon, 1998). Remarkably, the ER remains continuous throughout these reorganizations and maintains a resemblance of its original characteristic shape (Fig. 1 A). The ER is a dynamic organelle throughout the cell cycle in all organisms that have been imaged, yet it is still unclear whether ER dynamics play a critical role in ER functions, including protein secretion, lipid synthesis, and calcium regulation.

In animal cells, dynamic ER tubules coalign with microtubules (MTs), and ER dynamics are altered by depolymerization of MTs by cold-shock or the drug nocodazole (Terasaki et al., 1986; Waterman-Storer and Salmon, 1998). There are two mechanistically distinct ways that ER tubules can be visualized moving along MTs. The first mechanism is referred to as tip attachment complex (TAC) dynamics and describes the situation where the tip of the ER tubule appears attached to the tip of the MT plus end. During TAC, the ER tubule grows or retracts as its MT partner grows or retracts. TAC rearrangements occur on MTs that are dynamic and highly sensitive to nocodazole treatment (Waterman-Storer and Salmon, 1998). TAC rearrangements are dependent on an ER protein, STIM1, and an MT plus end–binding protein, EB1 (Grigoriev et al., 2008). STIM1 is also involved in calcium handling (Liou et al., 2007), but a link between these two functions has not been shown (Grigoriev et al., 2008), and the function of TAC remains undetermined.

The second mechanism of ER tubule dynamics is referred to as sliding, whereby the tip of the ER tubule initially binds to the shaft of an existing MT and slides along the MT as the ER tubule grows (Lee and Chen, 1988; Waterman-Storer and Salmon, 1998). Sliding does not correlate with MT growth or shrinkage. Sliding is less sensitive to nocodazole depolymerization of MTs than TAC (Waterman-Storer and Salmon, 1998), and its frequency is not affected by depletion of STIM1 or EB1 (Grigoriev et al., 2008). In addition, ER tubule sliding events are much more frequent and

J.R. Friedman and B.M. Webster contributed equally to this paper.

Correspondence to Gia K. Voeltz: gia.voeltz@colorado.edu

Abbreviations used in this paper: MT, microtubule; TAC, tip attachment complex; TSA, trichostatin A.

The Rockefeller University Press $30.00
J. Cell Biol. Vol. 190 No. 3 363–375
www.jcb.org/cgi/doi/10.1083/jcb.200911024

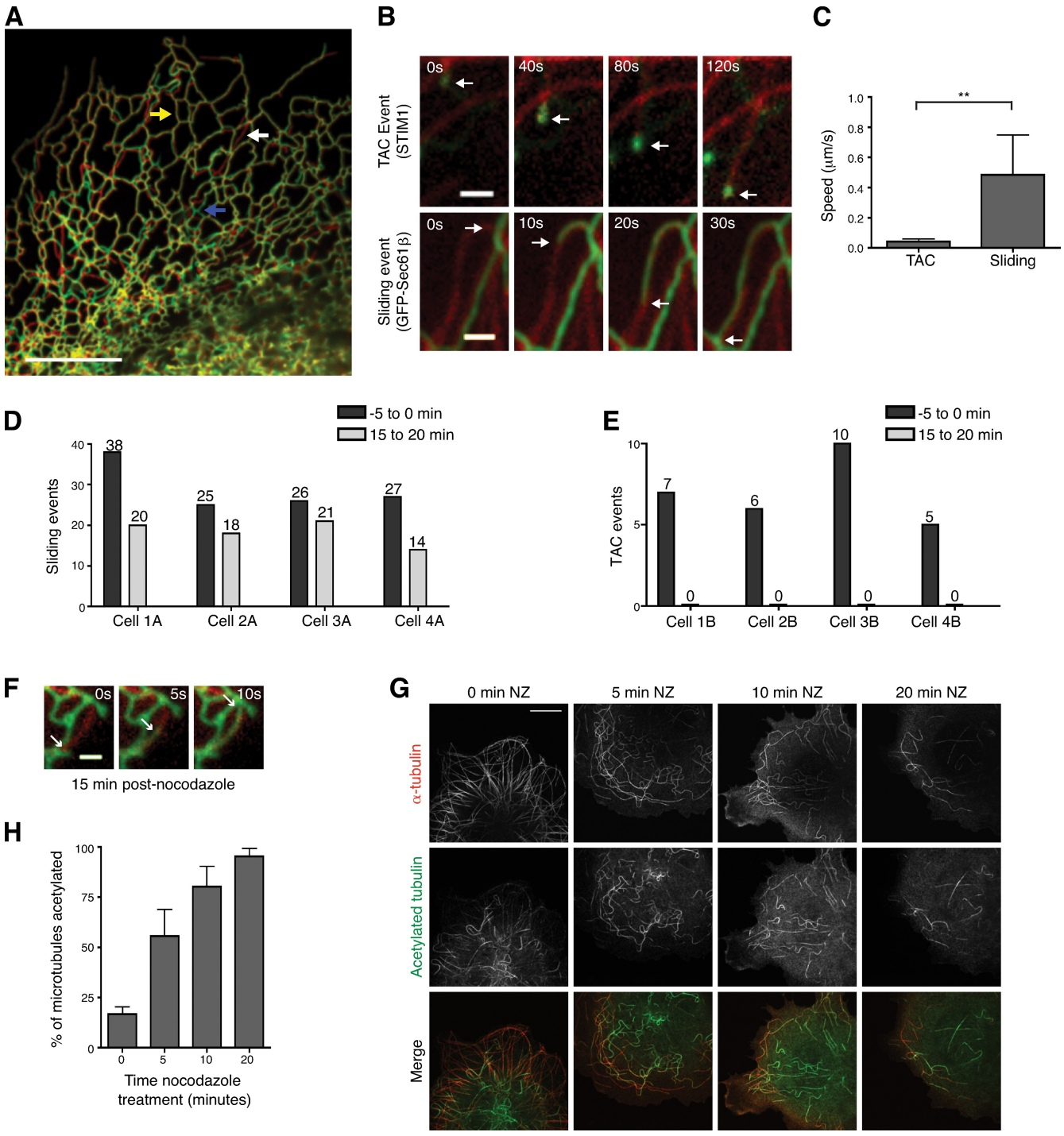

Figure 1. **ER sliding events occur on a nocodazole-resistant population of MTs, which is consistent with MT acetylation.** (A) Merged image of COS-7 cell expressing GFP–Sec61-β at t = 0 (green) and t = 30 s (red). Arrows indicate an unchanged ER position (yellow), a new sliding event (white), or a position of ER rearrangement (blue; see Video 1). (B) Examples of a TAC and sliding event (top and bottom panel, respectively). Dynamic events were captured by coexpressing mCherry–α-tubulin (red) and either YFP-STIM1 (TAC; green) or GFP–Sec61-β (sliding; green). Images shown are 10 s or 40 s apart for TAC versus sliding, respectively. Arrows indicate ER movement. (C) Graph of speed of TAC (n = 10) versus sliding events (n = 30). **, P = 4.3 × 10^{-10}; unpaired t test. (D) Number of sliding events longer than 1 μm in a 10 × 10–μm region during 5 min before and 15–20 min after 5 μM nocodazole treatment (n = 4 cells; see Videos 2 and 3). (E) Number of TAC events as in D in four different YFP-STIM1–expressing cells. (F) Example of an ER sliding event in a GFP–Sec61-β– and mCherry–α-tubulin–expressing cell 15 min after nocodazole treatment. Arrows depict the movement of an ER tubule along an MT. (G) Immunofluorescence staining of α-tubulin and acetylated tubulin in cells treated for 0, 5, 10, and 20 min with 5 μM nocodazole (NZ) before fixation. (H) Graph of the percentage of MTs containing acetylation staining over half of its length or >5 μm of its length at various times of nocodazole treatment (n = 3 cells per time point). (C and H) Error bars show standard deviation. Bars: (A and G) 10 μm; (B and F) 1 μm.

faster than TAC dynamics (Waterman-Storer and Salmon, 1998; Grigoriev et al., 2008). ER sliding occurs in both directions along MTs (Waterman-Storer and Salmon, 1998) and is thought to be driven by the MT-based motor proteins cytoplasmic dynein and kinesin-1 (Woźniak et al., 2009). No ER proteins have been identified that are responsible for ER sliding dynamics.

Why does the ER adopt a reticular network that is spread throughout the cell and why is this huge membrane-bound compartment constantly rearranging? Why do cells require two mechanisms to accomplish this? The ER contacts many other membrane-bound compartments in the cell, including mitochondria, lysosomes, Golgi, and the plasma membrane (Levine and Loewen, 2006; English et al., 2009). These interactions are functionally important for both lipid biosynthesis (Vance, 2008) and calcium signaling in animal cells (Csordás et al., 2006; de Brito and Scorrano, 2008) and may also be important for facilitating lipid transport. Because sliding and TAC are two mechanisms mediated by different factors and occurring at different rates, these mechanisms are likely important for different ER functions. To test how ER dynamics affect ER function, we must first understand which factors are involved.

In this study, we show that ER sliding occurs on stable MTs that have been posttranslationally modified by acetylation of α-tubulin subunits. In contrast, TAC occurs only on dynamic, nonacetylated, MTs. We propose that one reason that ER sliding occurs on acetylated MTs is to limit its distribution on defined paths within the cytoskeleton so that it can generate organelle contacts. We demonstrate that mitochondria, but not endosomes, are also preferentially found to colocalize with acetylated MTs. Together, these data suggest that ER sliding on acetylated MTs does not contribute to all interorganelle contacts; different organelles appear to rely on different MT modifications to contact the ER.

Results

TAC and sliding are unique mechanisms for ER travel along distinct populations of MTs

The ER network maintains a resemblance of its overall shape over time while constantly reorganizing its network of tubules and sheets. This is achieved in part by ER tubules growing, shrinking, and rearranging. These dynamics can be visualized by live imaging of COS-7 cells expressing the general ER marker GFP–Sec61-β (Fig. 1 A and Video 1). When images of the ER at different time points are merged (e.g., t = 0 [green] and t = 30 s [red] in Fig. 1 A), new tubules that formed during the 30-s time period are visualized in red (Fig. 1 A, white arrow), whereas ER regions remaining unchanged appear yellow (Fig. 1 A, yellow arrow). Regions where the ER has shifted or rearranged appear as green tubules in proximity to red ones (Fig. 1 A, blue arrow).

To address the mechanisms of MT-dependent ER dynamics, we first characterized the differences between tubule dynamics by TAC versus sliding. Cells were cotransfected with mCherry–α-tubulin (to visualize MTs) and either YFP-STIM1 (Liou et al., 2005; to mark ER TAC events) or GFP–Sec61-β (to visualize all ER dynamics). TAC events were those where the tip of the ER tubule was labeled with YFP-STIM1 and colocalized with the MT plus end tip (Fig. 1 B, top; Grigoriev et al., 2008). Sliding events were those whereby an ER tubule was initially bound to the MT shaft and slid along its length as the ER tubule extends (Fig. 1 B, bottom). We measured the relative speed and frequency of TAC versus sliding events and found that sliding was ∼10-fold faster than TAC (0.485 ± 0.264 µm/s vs. 0.044 ± 0.018 µm/s; Fig. 1 C), similar to data from HeLa cells (Grigoriev et al., 2008). Thus, TAC and sliding events differ in their speed of movement along MT tracts.

How do cells accomplish two mechanisms of ER motility? One possibility is that the two mechanisms occur on distinct MT populations. ER sliding dynamics were previously shown to be less sensitive than TAC dynamics to MT depolymerization with low levels of nocodazole (100 nM) in newt lung cells (Waterman-Storer and Salmon, 1998). We tested whether ER sliding in mammalian COS-7 cells is also less sensitive to 5 µM nocodazole. We measured the number of sliding or TAC events during 5-min windows before nocodazole treatment and 15–20 min after treatment (in a 10 × 10–µm box in the peripheral ER; Fig. 1, D and E; and Videos 2 and 3). We found that TAC events >1 µm in length ceased by 15 min after nocodazole treatment (Fig. 1 E). In contrast, sliding events decreased by <50% by 15–20 min after treatment (Fig. 1, D and F). By 60–65 min after treatment, ER sliding was nearly abolished. These results indicate that TAC events occur on dynamic MTs that are sensitive to nocodazole, whereas sliding events occur on MTs that are resistant to nocodazole.

Nocodazole-resistant MTs have been defined as the stable MTs, and this population has been shown to be marked by acetylation on lysine-40 of α-tubulin in 3T3 cells and rat astrocytes (Piperno et al., 1987; Cambray-Deakin et al., 1988). To quantify the correlation between nocodazole resistance and acetylation in COS-7 cells, the cells were treated with 5 µM nocodazole for increasing lengths of time, fixed, and stained with antibodies to both α-tubulin and acetylated α-tubulin, and the percentage of MTs that were acetylated was determined from the merged images. Our analyses focused on regions of the cell periphery where individual MTs could be resolved, and we counted an acetylated MT as one whose length appeared >50% acetylated or which contained >5 µm of acetylation staining (an arbitrary fluorescence intensity was used as a cutoff). At t = 0 (before nocodazole), only 17% of the MTs in the periphery appeared heavily acetylated (Fig. 1 G, left). Nocodazole treatment led to a dramatic and rapid reduction in the total number of MTs (Fig. 1 G, compare t = 0 with t = 10 min). Quite strikingly, of the MTs remaining at 10 min and 20 min after treatment, almost all were positive for acetylation (80% and 95%, respectively; Fig. 1 H). Therefore, acetylation marks a nocodazole-resistant population of MTs in COS-7 cells. Because sliding events are also resistant to nocodazole, collectively, these data suggest that ER sliding dynamics, and not TAC events, may preferentially occur on the subpopulation of MTs that are acetylated.

ER sliding events occur on acetylated regions of MTs

To directly test whether ER sliding occurs on acetylated MTs, we imaged live COS-7 cells that were cotransfected with GFP–Sec61-β and mCherry–α-tubulin on gridded coverslips and

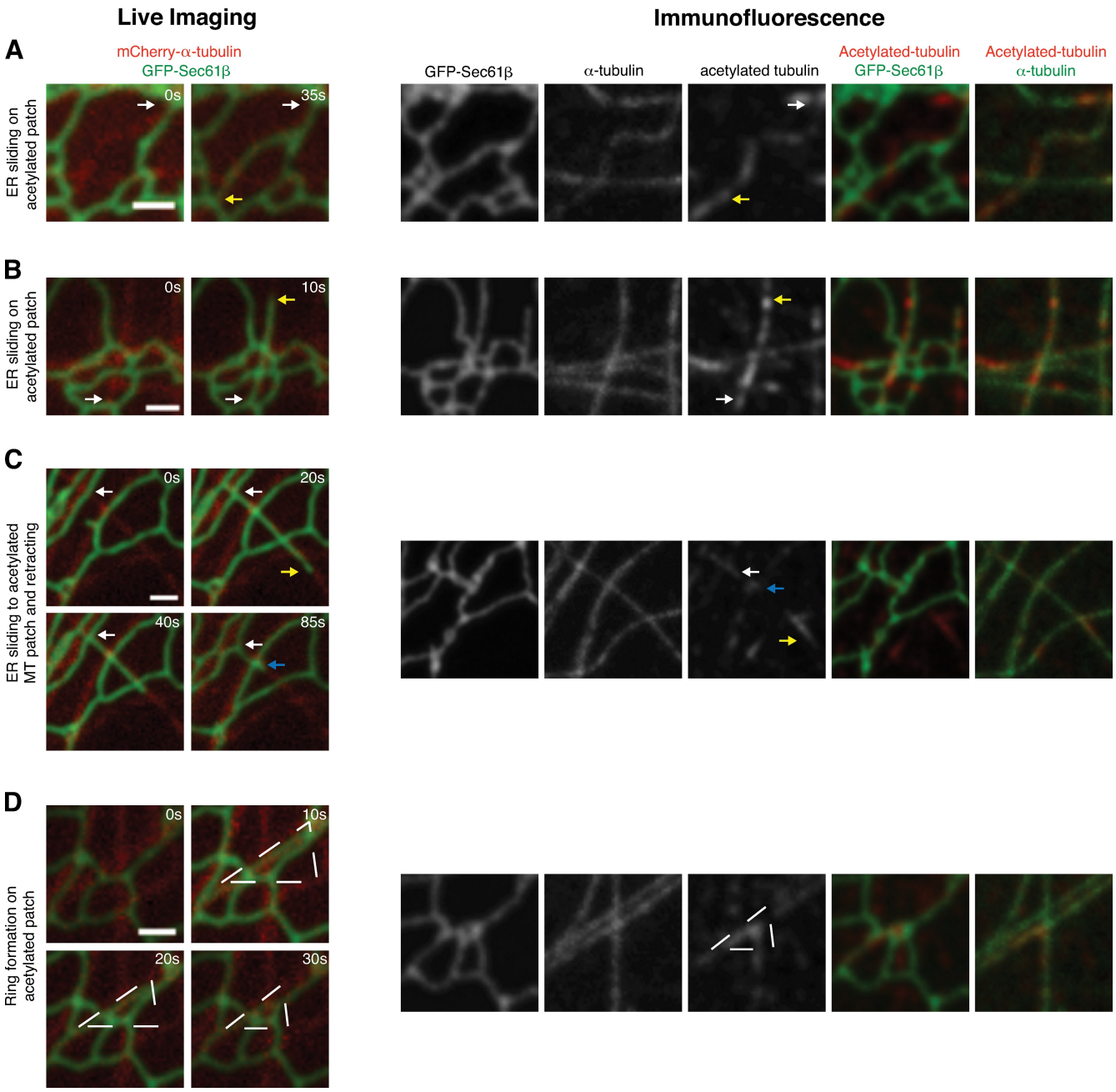

Figure 2. **Retrospective imaging demonstrates ER dynamics that occur on acetylated MTs.** (A–D, left) ER sliding events were captured during live cell imaging of cells expressing GFP–Sec61-β and mCherry–α-tubulin at the times indicated (in seconds). (right) Cells were then fixed and stained with antibody to α-tubulin and acetylated α-tubulin and reimaged. Merged images are shown with the indicated colors. (A and B) Examples of ER sliding on MTs with homogeneous acetylation staining. Sliding event progression during live imaging is marked with arrows for the starting position (white) and for end position (yellow). (C) An example of ER sliding from starting position (white arrows) to a patch of acetylation (yellow arrows) and retracting to a second acetylation patch (blue arrows). (D) An example of a sliding event, followed by an ER dynamic that leads to a ring formation (dashed triangles) around an acetylated MT patch. Bars, 1 µm.

quickly fixed the cells to preserve ER and MT structure. We then performed immunolabeling with antibodies to α-tubulin and acetylated α-tubulin and fluorescent secondary antibodies. The gridded coverslips allowed us to retrospectively identify the same cell that we imaged live.

Acetylation levels are not constant throughout the cell; the cell center contains more acetylated MTs than the periphery (Fig. S1). Likewise, the ER is most dense and the most dynamic in the perinuclear region. Yet, this density interferes with our ability to track single sliding events. Therefore, we focused on the periphery, where single ER sliding events are well resolved and can be retrospectively identified. In the periphery, many MTs have short stretches that stain positive for acetylation, which we refer to as acetylated patches.

As shown in Fig. 2 (A and B), ER sliding events along MTs (left) corresponded to regions along MTs that labeled positive for acetylation (right; for staining of entire cell, see Fig. S1). These events were identified because the ER and MTs were well

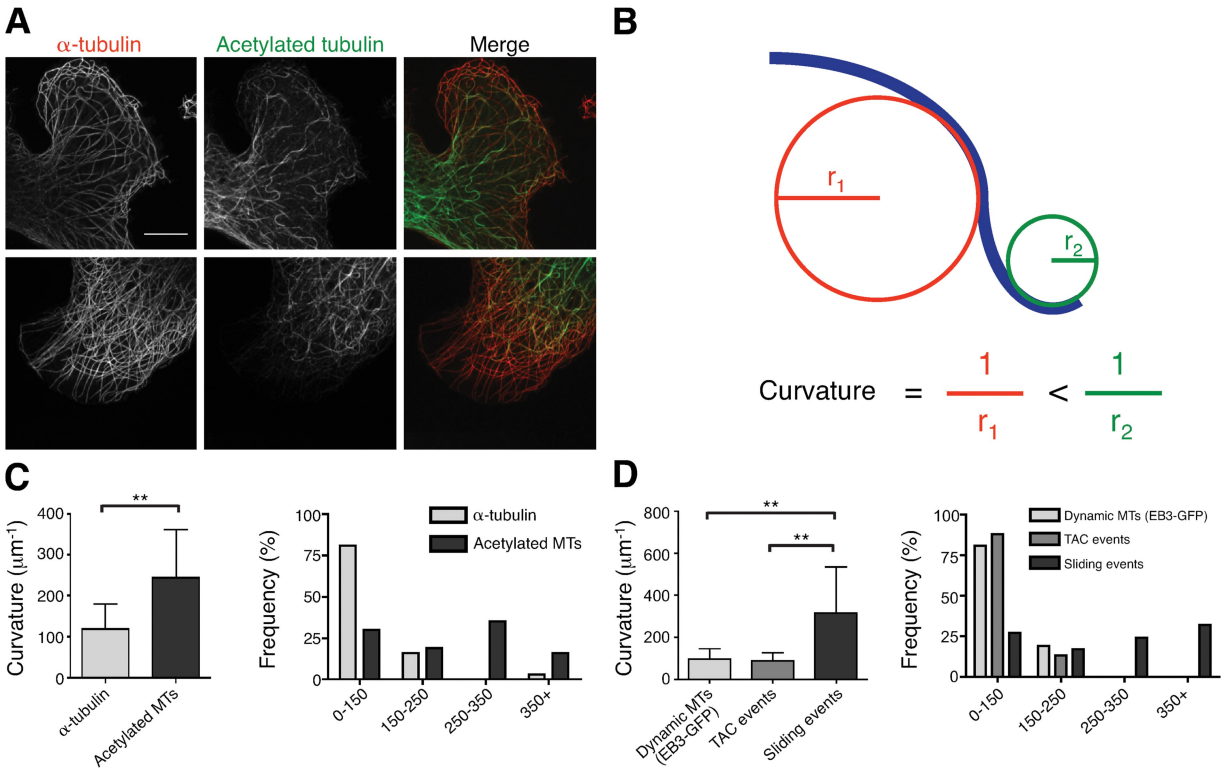

Figure 3. **Acetylated MTs and ER sliding events correlate with MT curvature.** (A) Immunofluorescence staining of α-tubulin and acetylated α-tubulin on untreated cells. (B) Diagram of curvature. (C, left) Graph of curvature of acetylated (n = 37) or nonacetylated MTs (n = 37). Acetylated MTs were picked by drawing a line through the cell at a point containing the maximum number of acetylated MTs. α-Tubulin staining of MTs that were not acetylated were picked along that line if they were isolated at the line. The mean curvature of the MT for 2.5 µm on either side of the line (or 5 µm total) was determined by "imodcurvature." (right) The frequency of MT curvature in groups of indicated values for nonacetylated MTs or acetylated MTs. (D) Curvature measurements for dynamic MTs (labeled with EB3; n = 37), TAC MTs (labeled with YFP-STIM1; n = 16), and ER sliding MTs (GFP–Sec61-β; n = 41). Right panel shows frequency of each event. (C and D) Error bars show standard deviation. P-values were determined by unpaired t test: **, $P = 3.7 \times 10^{-7}$ (C); and **, $P < 0.001$ (D). Bar, 10 µm.

resolved in that region of the cell, the sliding event clearly took place on a specific MT, the ER and MTs remained relatively static in place between the sliding event and fixation, and finally, MT acetylation staining was clearly positive for those examples. ER sliding events that occurred on acetylated MTs were also observed to undergo retractions (Fig. 2 C) as well as rearrangements into rings (Fig. 2 D).

Overall, the retrospective staining data suggest that ER sliding correlates with acetylation of the MT tracts. Quite strikingly, these events occurred on acetylated MT patches in a region of the cell periphery where acetylation is generally sparser. However, the inherent difficulties in retrospective imaging, including fixation and antibody access to antigen, as well as the uncertainties of how much signal constitutes an acetylated MT led us to develop a method for correlating the subpopulation of MTs that are acetylated with ER sliding in live cells.

Both MT acetylation and ER sliding correlate with MT curvature

While imaging acetylated MTs in cells treated with nocodazole (Fig. 1 G), we noticed that acetylated MTs appear much more curved than nonacetylated MTs. We reasoned that if ER sliding occurs preferentially on acetylated MTs and acetylated MTs are highly curved relative to nonacetylated ones, ER sliding should also occur at a higher frequency on MTs with high curvature.

To measure the curvature of acetylated versus nonacetylated MTs, cells were fixed and immunolabeled with antibodies to both α-tubulin and acetylated α-tubulin (Fig. 3 A). For quantification, we drew a line through a region of the cell periphery where individual MTs can be resolved and where the maximum number of heavily acetylated MTs appeared. For each acetylated and nonacetylated MT along that line (an arbitrary fluorescence intensity was used as a cutoff), the mean radius of curvature was calculated for a stretch 2.5 µm on each side of the line (Fig. S2 A) using the "imodcurvature" program from IMOD (Kremer et al., 1996). The radius of curvature at a point along a curve can be approximated by the radius of a circle that is fit to points along the curve (Bicek et al., 2007). For simplification, we will refer to the inverse of the mean radius of curvature as curvature. As seen in Fig. 3 B, the more curved an MT is, the smaller the radius of the circle and the larger the curvature will be.

We found that acetylated MTs have a significantly larger curvature (more than twofold greater) than nonacetylated MTs (244.6 μm^{-1} vs. 118.5 μm^{-1}; $n = 37$; $P = 3.7 \times 10^{-7}$; Fig. 3 C, left). However, more telling is the relative number of acetylated MTs that are highly curved. Only 3% of nonacetylated MTs counted had a curvature >250 μm^{-1}, whereas 51% of acetylated MTs had such a curvature (Fig. 3 C, right). These data suggest that MT curvature is a good indication for whether an MT is acetylated and provide a new method to predict MT acetylation in live cells.

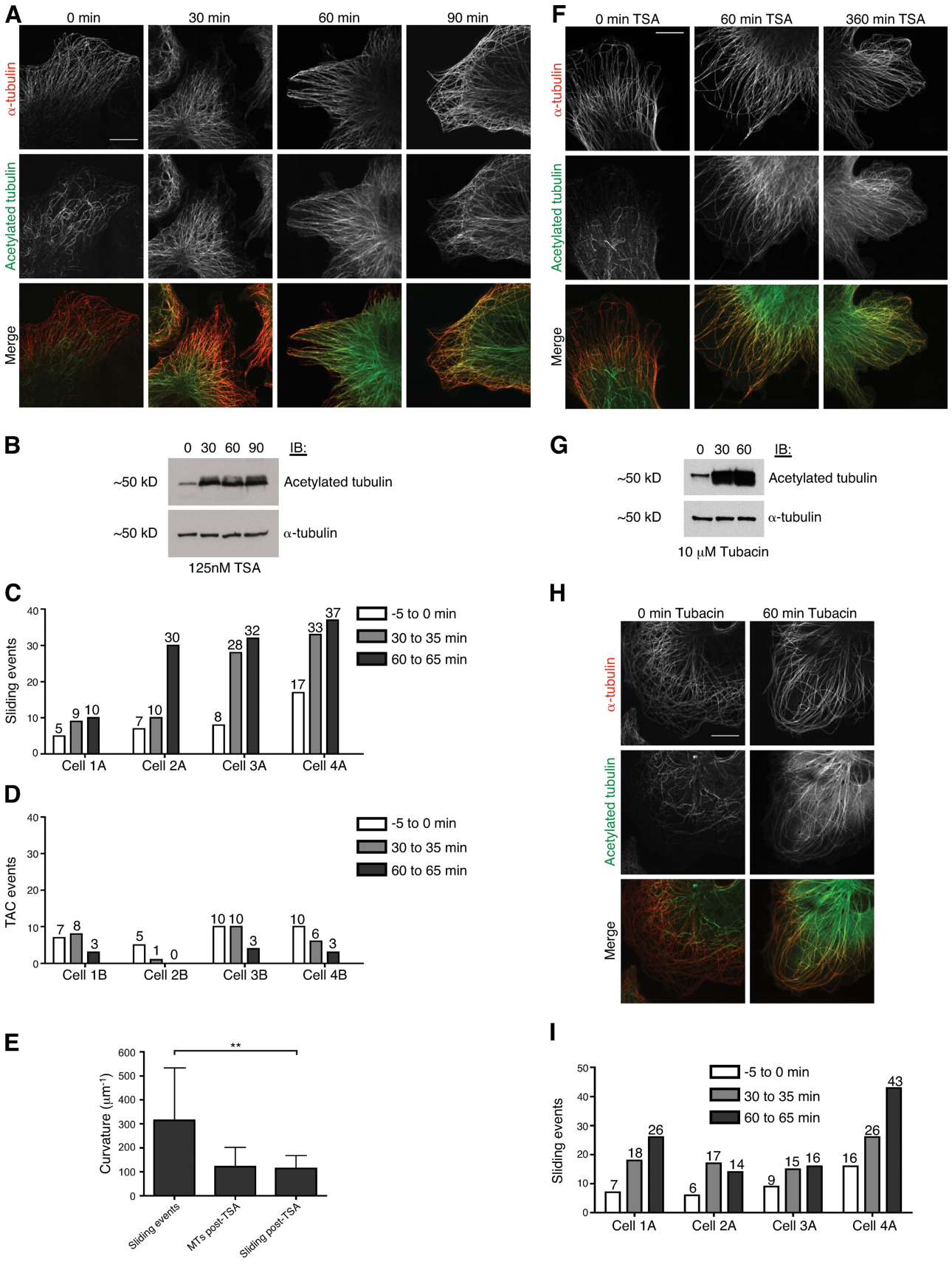

Figure 4. **Hyperacetylation of MTs by drug treatment increases ER sliding but not TAC events.** (A) COS-7 cells were fixed and immunofluorescently labeled with α-tubulin and acetylated α-tubulin after treatment with 125 nM TSA for 0, 30, 60, and 90 min. (B) COS-7 whole-cell lysate from cells treated for 0, 30, 60, and 90 min with 125 nM TSA were immunoblotted (IB) with antibodies to acetylated α-tubulin and α-tubulin. (C) Number of sliding events longer than

To correlate ER sliding events with MT curvature, we took live-cell videos of cells cotransfected with the ER marker GFP–Sec61-β and mCherry–α-tubulin and measured the curvature of MTs for sliding events that were longer than 2 µm. The mean curvature of these sliding events was 314.9 μm^{-1} ($n = 41$), and 56% of these events had a curvature >250 μm^{-1} (Fig. 3 D and Fig. S2 B). For comparison, we calculated the curvature of either dynamic MTs marked with the MT +TIP protein mCherry-EB3 (Stepanova et al., 2003) or mCherry–α-tubulin–labeled MTs that grew with the TAC ER protein YFP-STIM1. Dynamic MTs marked with EB3 had a mean curvature of 97.2 μm^{-1} ($n = 37$), and TAC events traveled on MTs with a mean curvature of 88.2 μm^{-1} ($n = 16$), which are both significantly lower than the curvature of MTs with sliding events ($P = 1.7 \times 10^{-7}$ and $P = 8.4 \times 10^{-8}$, respectively). These data suggest that ER sliding occurs along MTs that are acetylated and have a high curvature.

Increasing MT acetylation by drug treatment increases ER sliding

If ER sliding preferentially occurs on acetylated MTs, increasing the number of MTs that are acetylated should increase the number of ER sliding events. To test this, we added trichostatin A (TSA; at 125 nM), a drug which is a general inhibitor of the HDAC (histone deacetylase) family of deacetylases, including HDAC6 (Koeller et al., 2003). HDAC6 is a cytoplasmic deacetylase responsible for removing the acetylation modification from MTs (Hubbert et al., 2002; Reed et al., 2006). Cells were treated for increasing amounts of time with TSA, fixed, and immunolabeled with antibodies to fluorescently label α-tubulin and acetylated α-tubulin (Fig. 4 A). By 30 min after TSA treatment, acetylation staining marked almost all of the MTs in the cell. This corresponds to the increase in the levels of acetylated tubulin seen by immunoblotting (Fig. 4 B, top). Note that the overall levels of α-tubulin did not change (Fig. 4 B, bottom).

We then measured whether the increase in MT acetylation corresponded to an increase in sliding events; we counted the number of sliding events >1 µm in length in a 10 × 10–µm box during a 5-min period before treatment and 30–35 and 60–65 min after TSA treatment. In each case, the number of sliding events in the region increased two- to fourfold between 0 and 60 min ($n = 4$ different cells; Fig. 4 C and Videos 4 and 5). As a control, we tested whether the number of TAC events, marked with YFP-STIM1, increased after TSA treatment. In contrast to sliding, the frequency of TAC events longer than 1 µm in four cells decreased over the same period of TSA treatment (Fig. 4 D). The increased amount of sliding that occurs after TSA treatment provides a direct link between ER sliding events and the level of MT acetylation in the cell.

Because under normal conditions acetylated MTs are more curved than nonacetylated MTs (Fig. 3 C), we predicted that the hyperacetylated MTs generated by TSA treatment would also be curved. However, hyperacetylation does not cause an increase in overall levels of MT curvature (Fig. 4, A and E). Because TSA treatment causes MTs that were previously nonacetylated and straight to become acetylated and straight, we can then ask whether ER sliding after TSA treatment occurs at a higher rate on straight MTs. To test this, we imaged sliding events between 60 and 90 min after TSA treatment and measured the curvature of the MTs from these events. Indeed, the mean curvature of sliding events in TSA-treated cells was 114.4 μm^{-1} ($n = 30$; Fig. 4 E and Fig. S2 C), which is significantly different from the curvature of sliding events from untreated cells measured in Fig. 3 (314.9 μm^{-1}; $P = 1.0 \times 10^{-6}$).

To test whether the curvature of sliding events after TSA treatment is similar to the mean curvature of the overall MT population, we drew a 5-µm-wide box across the cell periphery of a representative cell treated with TSA and measured the mean curvature of every MT in this box. The curvature of this population of MTs was 121.7 μm^{-1} ($n = 35$; Fig. 4 E and Fig. S2 C), which is comparable with the curvature of sliding events after TSA treatment (114.4 μm^{-1}). Therefore, ER sliding does not have a preference for curved acetylated MTs when compared with straight MTs that are also acetylated. Together, these data further support the idea that ER sliding favors MTs that are marked by acetylation because ER sliding occurs on acetylated MTs even when they are not curved. Although MTs from cells treated for 60 min with TSA do not appear more curved, we hypothesized that perhaps newly acetylated MTs will become curved over a long period of time. However, the hyperacetylated MTs were still not significantly more curved even 6 h after TSA treatment (Fig. 4 F).

To verify that the effect of TSA treatment on ER sliding was caused by the inhibition of HDAC6 rather than another member of the HDAC family, we treated cells with a structural analogue of the drug tubacin, a specific inhibitor of HDAC6 (Haggarty et al., 2003). Treatment of COS-7 cells with 10 µM tubacin increased MT acetylation by both immunoblot and immunofluorescence (Fig. 4, G and H, respectively) in a manner and scale similar to TSA, and sliding events also increased in number at a rate similar to TSA (Fig. 4 I). These results demonstrate that the effect on ER sliding is specifically caused by inhibition of HDAC6, the MT deacetylase.

The function of ER sliding is not known. One possible role of ER sliding would be to allow the ER to probe the cytosol to form contacts with other cytoplasmic membrane-bound compartments. By immunofluorescence staining, only 17% of MTs in the cell periphery appear heavily acetylated along the majority of their length (Fig. 1 H). Some MTs that are not heavily acetylated throughout their length have patches of acetylation, which also appear in our imaging experiments to serve as regions for ER sliding (Fig. 2). Densitometric analysis of immunoblots showed that both TSA and tubacin treatment increased MT acetylation by four- to sixfold relative to all tubulin (Fig. 4, B and F), indicating

1 µm in a 10 × 10–µm region during 5-min period before and 30–35 and 60–65 min after treatment with 125 nM TSA ($n = 4$ different GFP–Sec61-β–expressing cells; see Videos 4 and 5). (D) Number of TAC events, as in C, in four different YFP-STIM1–expressing cells. (E) Graph of the curvature of ER sliding events (GFP–Sec61-β) from 60–90 min after 125 nM TSA treatment ($n = 30$) as compared with ER sliding curvature from Fig. 3 and the curvature of a representative population of MTs from a cell treated for 60 min with TSA ($n = 35$). Error bars show standard deviation. P-value was determined by unpaired *t* test: **, $P < 0.001$. (F) As in A, cells were treated for 0, 1, and 6 h with TSA. (G–I) As in A–C for cells treated with 10 µM tubacin. Bars, 10 µm.

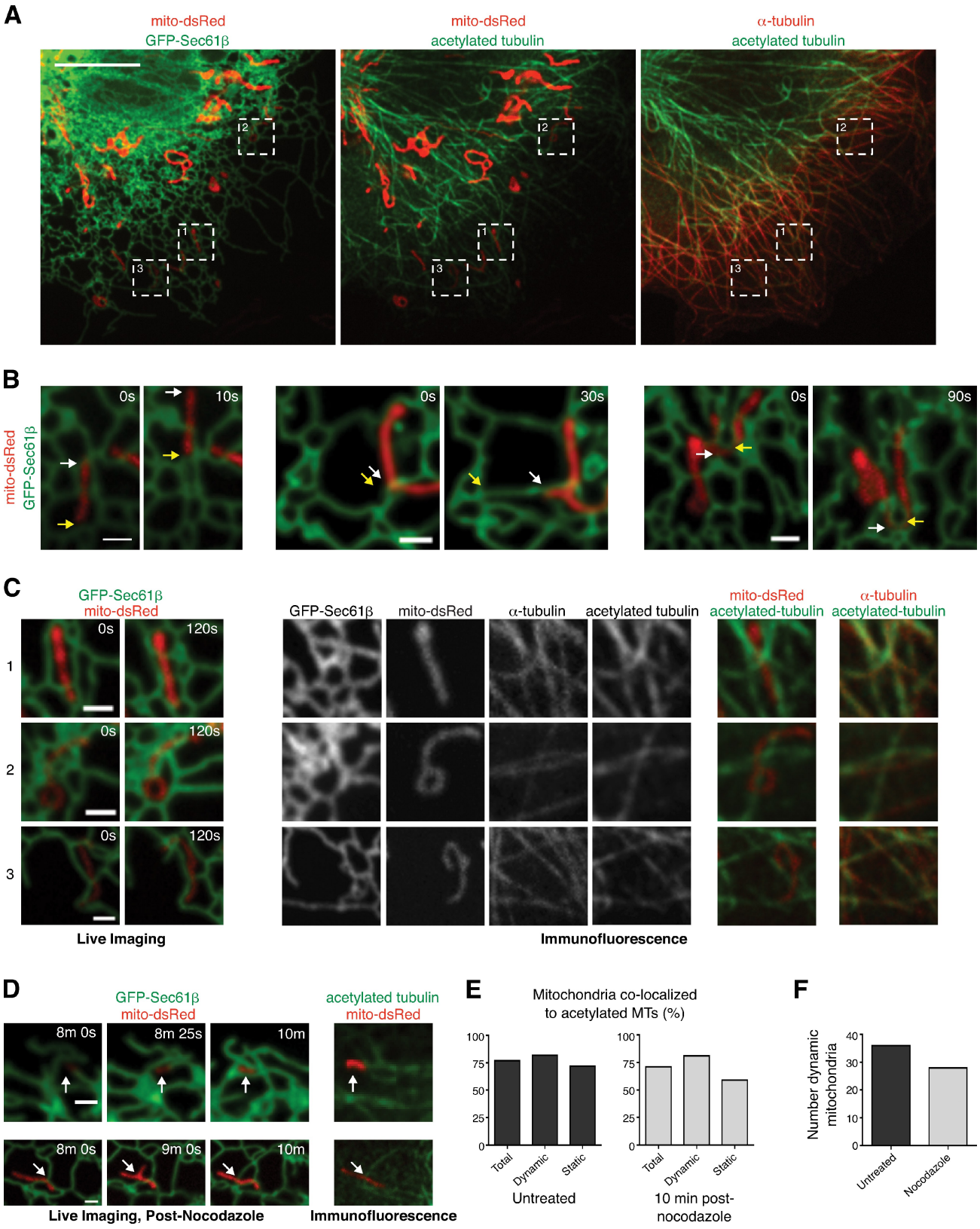

Figure 5. **ER and mitochondria dynamics are coupled, and mitochondrial localization is enriched on acetylated MTs.** (A) Merged image of a COS-7 cell showing colocalization of mito-dsRed and GFP–Sec61-β (left), mito-dsRed and immunolabeled for acetylated α-tubulin (middle), and immunolabeled for α-tubulin and acetylated α-tubulin (right). Dashed boxes indicate mitochondria imaged in C. (B) Time-lapse of ER–mitochondria interactions in cells expressing GFP–Sec61-β and mito-dsRed at the times indicated (see Videos 6–8). Left panel shows an ER tubule moving behind a mitochondrion. Middle panel shows a mitochondrion moving behind an ER tubule. Right panel shows massive co-rearrangement of both. Arrows indicate the position of mitochondrion (white) or ER (yellow) at each time point. (C, left) As in B. (right) Cells were fixed, immunolabeled with antibodies to α-tubulin and acetylated α-tubulin, and reimaged. Images were merged and shown with indicated colors. (D) As in C, except cells were imaged between t = 8 and t = 10 min after 5 μM

that no more than 25% of tubulin subunits are acetylated in COS-7 cells (as well as HeLa and U2OS cells; Fig. S3). Because ER sliding dynamics preferentially occur on the subset of MTs that are acetylated, we predicted that contacts with other organelles might occur at a higher frequency if other organelles are also preferentially bound to and/or moving on acetylated MTs.

ER and mitochondrial dynamics are coupled

Mitochondria interact physically with the ER (Staehelin, 1997; Rizzuto et al., 1998; Perktold et al., 2007; de Brito and Scorrano, 2008; Kornmann et al., 2009), and this interaction is important for both lipid synthesis and calcium handling (Csordás et al., 2006; Vance, 2008). Mitochondria have been reported to colocalize with acetylated MTs in rat astrocytes (Cambray-Deakin et al., 1988) and thus were a good candidate to test our model. Mitochondria and ER are both dynamic organelles, but it is not clear how much contact they maintain while both organelles are moving. To address this, COS-7 cells were cotransfected with the ER marker GFP–Sec61-β and a mitochondrial marker, mito-dsRed (Song et al., 2009), and imaged live to visualize the contacts between these two organelles. The mitochondria are quite variable in their morphology and dynamics (Boldogh and Pon, 2007; Frederick and Shaw, 2007). In COS-7 cells, the mitochondria exist as long branched ribbons, short tubules, donuts, and spheres; they also range from being static over time to moving quite rapidly. However, every mitochondrion we visualized (we focused on those in the cell periphery because the ER is nicely resolved) appeared to be in direct contact with the ER at all times at the resolution of fluorescence microscopy (Fig. 5 A, left). The interactions between the ER and mitochondria are maintained despite the common dynamic rearrangements experienced by both organelles. These coupled dynamics fall into three categories: (1) an ER tubule moves behind a dynamic mitochondrion, (2) a mitochondrion moves behind a dynamic ER tubule, and (3) most commonly, the ER is wrapped around a mitochondria ribbon, and the two organelles move together with rearrangements of both (Fig. 5 B and Videos 6–8). These images show that the dynamics of the mitochondrion (Fig. 5 B, white arrows) along with the corresponding dynamics of the ER (Fig. 5 B, yellow arrows) are tightly interrelated and interconnected and can be maintained when both organelles are moving. In fact, even after treatment with ionomycin, a drug which disrupts calcium regulation and the morphology of ER (Subramanian and Meyer, 1997) and mitochondria (Hom et al., 2007), the vesiculated ER and mitochondria remained in contact although both organelles were fragmented (Fig. S4).

Mitochondria preferentially localize to regions of MT acetylation

We find that every mitochondrion remains localized to the ER during their coupled dynamics (Fig. 5 B and Videos 6–8). If acetylated MTs play a role in directing or maintaining ER–mitochondrial contact, we predicted that the two organelles would be found in contact over regions of MTs that are acetylated. To test this, cells were cotransfected with GFP–Sec61-β and mito-dsRed and imaged live on gridded coverslips and then quickly fixed and retrospectively immunolabeled for α-tubulin and acetylated MTs. We show images of the ER and mitochondria from one fixed cell with typical and representative acetylation staining (Fig. 5 A). Shown in Fig. 5 C are time-lapse images of three examples (Fig. 5 A, white dashed boxes) of mitochondrial ribbons that remain fairly stationary over at least 2 min and also maintain their interaction with the ER. The right panels show images of these cells after fixation by immunofluorescence. When looking at the entire cell, mitochondrial localization correlates well with areas that have the most MT acetylation (Fig. 5 A). We quantified the percentage of mitochondria that colocalized with acetylated MTs to be 77% (n = 57 mitochondria from 10 cells; Fig. 5 E, left). We next measured whether dynamic mitochondria also colocalized at a high frequency along acetylated MTs. Indeed, 23 of the 28 (82%) dynamic mitochondria we imaged retrospectively appeared to colocalize to acetylated MTs (Fig. 5 E, left).

We also visualized colocalization between mitochondria and acetylated MTs after 5 µM nocodazole treatment (10 min) to depolymerize the bulk of nonacetylated MTs and improve our visualization of the acetylated MTs (same conditions as shown in Fig. 1 [G and H]). We reasoned that if the mitochondria were bound to acetylated MTs, their position would not be expected to drift significantly relative to the acetylated MTs after the nonacetylated MTs were depolymerized. Mitochondria dynamics were imaged (from t = 8 until t = 10 min after the addition of 5 µM nocodazole), and cells were fixed and retrospectively immunolabeled. Similar to our observation in untreated cells, 71% of all mitochondria in the cell periphery colocalized with MTs that were acetylated even after nocodazole treatment (n = 48 mitochondria from 8 cells; Fig. 5 E, right). The percentage was higher for dynamic mitochondria: 21 out of 26 dynamic mitochondria colocalized with acetylated MTs (81%; two examples are shown in Fig. 5 D and Videos 9 and 10). Together, these data demonstrate that the majority of both static and dynamic mitochondria localize to at least one acetylated MT.

Mitochondrial dynamics are also relatively insensitive to nocodazole-induced MT depolymerization. Of 36 dynamic mitochondria that were discernable both before and after nocodazole, 28 remained dynamic 10 min after nocodazole (78%; Fig. 5 F). At this time point, the vast majority of those MTs that remained were acetylated (>80%; Fig. 1 H). We show two examples of mitochondria that moved along an acetylated MT after nocodazole treatment by retrospective imaging (Fig. 5 D). However, although these data are good evidence that mitochondria can move on the acetylated MTs that they are localized to,

nocodazole treatment (see Videos 9 and 10). (top) Arrows mark an ER tubule moving behind a dynamic mitochondrion; after fixation it colocalizes with acetylated MTs. (bottom) Arrows mark where a dynamic mitochondria tubule grows and retracts, followed by a growing ER tubule on an acetylated MT. (E) Percentage of mitochondria that retrospectively colocalize to sites of MT acetylation in untreated cells (77% of 57 total, 72% of 29 static, and 82% of 28 dynamic mitochondria from 10 cells; left) and cells treated for 10 min with 5 µM nocodazole (71% of 48 total, 59% of 22 static, and 81% of 26 dynamic mitochondria from 8 cells; right). (F) Total number of mitochondria from the experiment described in D that are dynamic before (dark gray; n = 36) versus after nocodazole treatment (light gray; n = 28). Bars: (A) 10 µm; (B–D) 1 µm.

it is not clear whether acetylation regulates mitochondrial movement to the same extent as it does the ER because TSA treatment does not increase mitochondrial dynamics (Fig. S5). Regardless, a large percentage of mitochondria colocalized to regions of MT acetylation, which supports the notion that ER sliding on acetylated MTs may establish and/or help maintain the integrity of this interorganelle contact.

Endosome–ER contacts are enriched on MTs that are not acetylated

Because ER sliding and mitochondrial contacts colocalize prevalently to acetylated MTs, we wanted to test whether this is a phenomenon particular to all organelles in contact with the ER. Endosomes are a dynamic organelle in the cell and have been shown to contact the ER (Rocha et al., 2009; Eden et al., 2010). To visualize endosomes, we generated a construct expressing mCherry fused to an early endosomal marker, Rab5 (Rink et al., 2005). Endosomes mostly appear as puncta and can be seen distributed throughout the cell cytoplasm (Fig. 6 A). A large percentage of early endosomes appear in contact with the ER at the resolution of fluorescence microscopy, and these contacts are maintained despite ER and endosome rearrangements and dynamics reminiscent of ER–mitochondrial contacts. We show three examples of ER–endosome contacts over time in Fig. 6 B.

To test whether early endosomes and ER–endosome contacts occur preferentially on regions of the MTs that are acetylated, we fixed cells expressing GFP–Sec61-β and mCherry-Rab5 and stained by immunofluorescence for both acetylated α-tubulin and α-tubulin. We then merged images of endosomal puncta with images showing all MTs and acetylated MTs in cells with typical acetylation staining (Fig. 6 C). We tested the colocalization of 426 early endosomes with both MTs and the ER in five different cells in the cell periphery where the ER could be resolved. We counted 238 endosomes (56% of total) that colocalized with MTs and 266 endosomes (62% of total) that colocalized with the ER (Fig. 6 D). Although these numbers may vary from cell to cell, the extent to which early endosomes contact the ER is quite significant.

We then determined the percentage of the endosomes that are localized to acetylated MTs. Of the 238 MT-localized endosomes, only 61 (26%) localized to acetylated MTs (Fig. 6 E). We also tested whether the endosomes that are specifically ER localized are found at a higher rate on acetylated MTs. We identified 162 endosomes (38% of 426 total) that localized to the ER and MTs. Of these, only 47 were on acetylated MTs (29% of the 162), which is only slightly higher than the value for all endosomes (Fig. 6 E). One possible explanation is that as endosomes are trafficked to the ER, a small percentage reaches parts of the ER that are localized to acetylated MTs. Interestingly, 18% of endosomes that are on MTs, but not ER localized, align with acetylated MTs (Fig. 6 E). Together, these data suggest that early endosomes do not have a preference for acetylated MTs and are therefore unlikely to be using acetylated MTs as a primary method to establish or maintain contact with the ER membrane.

As with mitochondria, we treated cells with 5 µM nocodazole for 10 min to improve our visualization of acetylated MTs. We counted a total of 443 endosomes from five cells fixed after nocodazole treatment, and 11% of all endosomes and 15% of ER-localized endosomes localized to acetylated MTs, compared with 14% and 18%, respectively, in untreated cells (Fig. 6 F). These data demonstrate by two methods that only a small percentage of endosomes localize to acetylated MTs.

Thus, the frequency of endosome–ER contacts on acetylated MTs is much rarer than that of ER–mitochondrial contacts and matches the distribution that would be expected if the endosomes had no preference for acetylated MTs. Together, these data suggest that MT acetylation may be a mechanism by which the ER can establish and/or maintain contact with mitochondria but not endosomes.

Discussion

The ER travels along MTs by two distinct mechanisms in the cell, TAC and sliding. Sliding events are much faster than TAC, are far more prevalent in the cell (5–10-fold), and occur on a subset of MTs that are resistant to nocodazole. However, until recently, the mechanism behind ER sliding events had been largely unexplored. In this study, we show that ER sliding events occur preferentially on acetylated MTs. After nocodazole treatment, TAC events stop before sliding events, and sliding events persist when almost all remaining MTs in the cell are acetylated. Additionally, ER sliding events can be retrospectively imaged to occur on acetylated MTs. Furthermore, both acetylated MTs and the MTs on which sliding events occur are highly curved when compared with both nonacetylated MTs and dynamic MTs, respectively. Finally, increasing the amount of MT acetylation in the cell by drug treatment increases the amount of ER sliding but not TAC events. Although acetylated MTs have been previously shown to be involved in axonal and neurite transport (Reed et al., 2006; Hammond et al., 2010) and have a potential role in ciliogenesis (Loktev et al., 2008), this is the first direct function that has been shown for acetylated MTs in the cytoplasm of an epithelial cell.

Why would ER sliding occur preferentially on the subset of MTs that are acetylated? Why do cells have different populations of MTs? We hypothesize that ER dynamics occur on acetylated MTs to stimulate ER–ER fusion and ER–mitochondrial contacts. ER interactions with mitochondria are important for both lipid synthesis and calcium handling in the cell; however, little is known about how the ER and mitochondrial membranes establish productive contact in the vast cell cytoplasm. Every mitochondrion we looked at was already in contact with the ER, and our live-imaging data demonstrate quite clearly that mitochondria–ER contact sites are maintained even despite the dynamics experienced by both organelles. Our retrospective videos reveal that both dynamic and static mitochondria localize to acetylated MTs, which supports a model that one function of ER sliding on acetylated MTs could be to establish and/or maintain contact with mitochondria. ER dynamics are strikingly more frequent in general than mitochondrial dynamics, and so it is likely that the ER finds the mitochondria and not vice-versa.

Like mitochondria, Rab5-positive early endosomes are often in contact with the ER even during ER dynamics; however, endosomes do not preferentially localize to acetylated MTs. Of the population of endosomes that do not localize to the ER

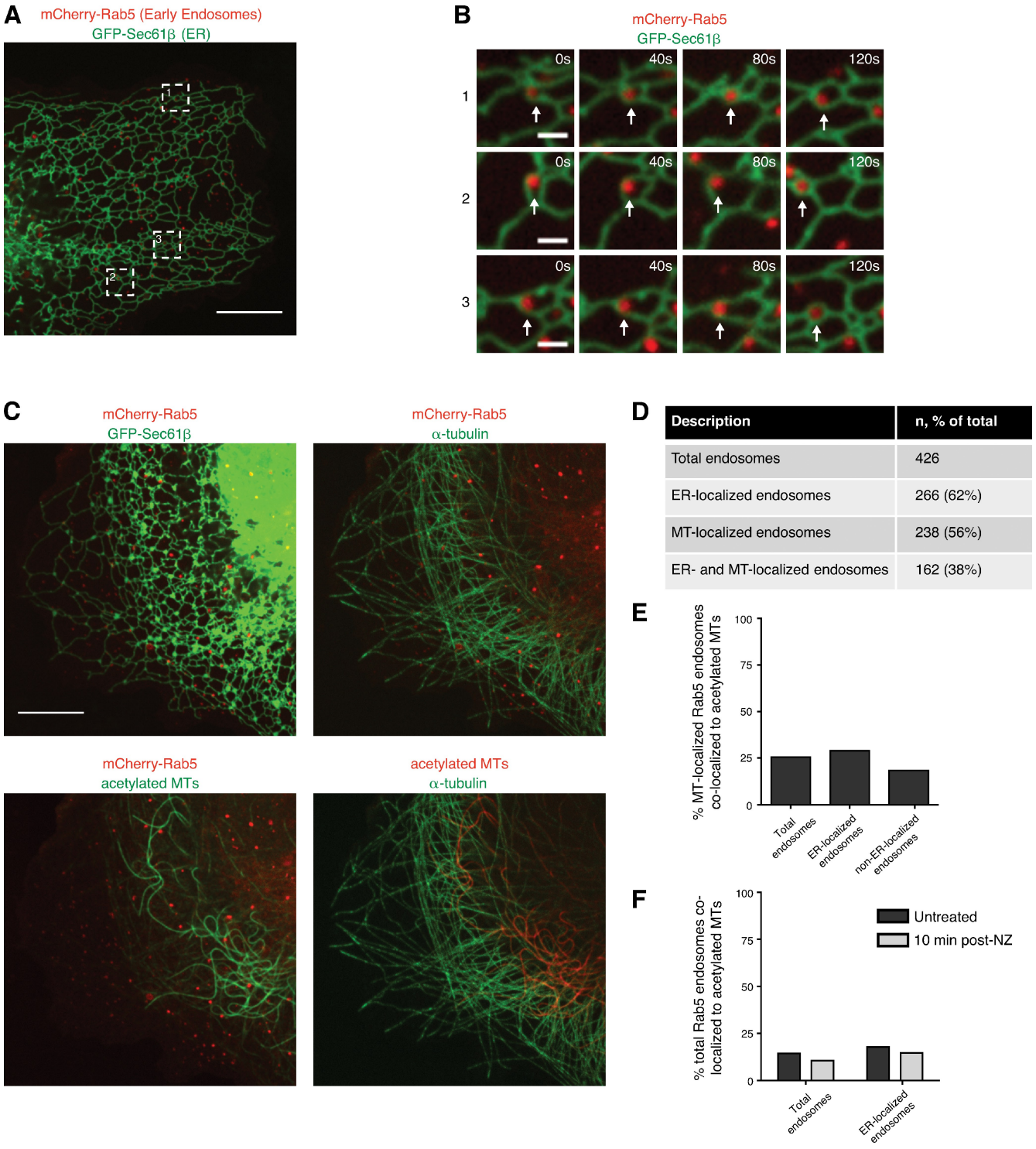

Description	n, % of total
Total endosomes	426
ER-localized endosomes	266 (62%)
MT-localized endosomes	238 (56%)
ER- and MT-localized endosomes	162 (38%)

Figure 6. **Early endosomes that interact with the ER are not enriched on acetylated MTs.** (A) Merged image of a COS-7 cell showing colocalization of mCherry-Rab5 and GFP–Sec61-β. Dashed boxes indicate early endosomes imaged in B. (B) Time-lapse images of ER–endosome interactions in cells expressing GFP–Sec61-β and mCherry-Rab5 at the times indicated. Arrows indicate the position of the endosome at each time point. (C) Merged images of a fixed COS-7 cell expressing GFP–Sec61-β and mCherry-Rab5 and immunolabeled for α-tubulin and acetylated α-tubulin. Images shown are merges for the indicated labels. (D) Table indicating localization of endosomes to ER and MTs. (E) Percentage of MT-localized endosomes that colocalize to acetylated MTs. Left bar is total MT localized (n = 61 of 238; 26%), middle bar is ER and MT localized (n = 47 of 162; 29%), and right bar is MT and non-ER localized (n = 14 of 76; 18%) from five cells. (F) Percentage of endosomes that colocalize with acetylated MTs before (dark gray) and 10 min after (light gray) 5 µM nocodazole (NZ) treatment. Left bars are all endosomes (untreated n = 61 of 426 [14%] from five cells; nocodazole-treated n = 47 of 443 [11%] from five cells). Right bars are ER localized (untreated n = 47 of 266 [18%]; nocodazole-treated n = 29 of 198 [15%]). Bars: (A and C) 10 µm; (B) 1 µm.

but do localize to the MTs, only 18% are on acetylated MTs. Therefore, these endosomes are unlikely to preferentially use acetylated MTs to find the ER membrane. A relevant difference between endosomes and mitochondria or the ER is that endosome movements have been shown in vivo to occur via a kinesin-3 family member (KIF16B; Hoepfner et al., 2005), whereas mitochondria and ER have been shown to traffic using kinesin-1 (Hurd and Saxton, 1996; Tanaka et al., 1998; Woźniak et al., 2009). Interestingly, kinesin-1 has been shown to have a preference for acetylated MTs in COS cells, whereas a kinesin-3 family member, KIF1A, does not (Cai et al., 2009). Together, these data suggest that different organelles contact the ER through different mechanisms that may be determined by which kinesin motor protein they use to bind to MTs.

The proteins responsible for MT acetylation have not yet been discovered, but their identity would be helpful for testing the functionality of ER sliding and ER–mitochondrial coupling. Identifying the ER proteins that link the sliding ER tubule to kinesin-1 on acetylated MTs will also be crucial for understanding the role of ER dynamics. Multiple ER proteins that bind MTs have been identified that may be responsible (Vedrenne and Hauri, 2006) and now can be tested for their colocalization with acetylated MTs. Furthermore, although we have touched on one potential function of ER sliding as to establish and maintain contact with mitochondria, we assume that it could also play a role in trafficking and aid in the dispersion of ER components throughout the cytoplasm. It remains to be tested whether Golgi and COP (coat protein complex) vesicles are also localized to acetylated MTs. Our experiments measured colocalization between the ER and Rab5-labeled endosomes, and we did not see enrichment on acetylated MTs. However, Rab5 endosomes are considered early endosomes, and future experiments will need to address whether late or recycling endosomes colocalize with the ER on acetylated MTs. One clue would be if the structure and or dynamics of these organelles have only partial sensitivity to nocodazole treatment and colocalize with curved MTs.

Materials and methods

Constructs and antibodies

YFP-STIM1 was a gift from T. Meyer (Stanford University, Palo Alto, CA) via A. Palmer (University of Colorado at Boulder, Boulder, CO). Mito-dsRed was a gift from D. Chan (California Institute of Technology, Pasadena, CA). mCherry-EB3 plasmid was a gift from N. Galjart (Erasmus Medical Center, Rotterdam, Netherlands). mCherry–α-tubulin was generated by substituting mCherry for EYFP in EYFP–α-tubulin (Takara Bio Inc.). GFP–Sec61-β was previously described (Voeltz et al., 2006). mCherry-Rab5 was a gift from A. English (University of Colorado at Boulder) and was generated by cloning mCherry into the NheI–BglII sites of pAcGFP1-N1 (Takara Bio Inc.) and cloning human Rab5b followed by a stop codon into the BglII–KpnI sites of that vector. Antibody to acetylated α-tubulin for immunofluorescence and Western blotting was purchased from Sigma-Aldrich (6-11B-1). Antibody to α-tubulin for immunofluorescence was purchased from Abcam. Antibody to α-tubulin used for Western blotting was purchased from Cell Signaling Technology (11H10).

Cell culture, transfection, and drug treatments

COS-7 cells (American Type Culture Collection) were grown in DME supplemented with 10% FBS and 1% penicillin/streptomycin. Cells were seeded at 2×10^5 cells per well of a 6-well dish for transient transfection. Transfections were performed in OPTI-MEM medium (Invitrogen) with 5 µl Lipofectamine 2000 (Invitrogen) and the following amounts of plasmid DNA: 1–2 µg GFP–Sec61-β, 200 ng YFP-STIM1, 125 ng mCherry–α-tubulin, 50 ng mCherry-EB3, 50 ng mito-dsRed, and 1 µg mCherry-Rab5. Cells were returned to fresh growth medium 5 h after transfection and were split 24 h after transfection onto 35-mm glass-bottom microscope dishes or glass-bottom gridded microscope dishes (MatTek) at a density of 2×10^5 cells per dish and allowed to adhere for at least 4 h. Before live-cell imaging, cell medium was changed to OPTI-MEM medium. During drug treatment, cells were treated with 5 µM nocodazole (Acros Organics), 125 nM TSA (Sigma-Aldrich), 10 µM tubacin MAZ1370 (provided by R. Mazitschek and S. Schreiber, Broad Institute, Cambridge, MA), or 2 µM ionomycin (Invitrogen).

Immunofluorescence

Cells were fixed with 4% paraformaldehyde (EMS) and 0.5% glutaraldehyde (EMS) for 15 min in PBS and permeabilized in 0.1% Triton X-100 (Thermo Fisher Scientific) in PBS for 5 min. Cells were stained with the indicated primary antibodies and corresponding anti–mouse or anti–rabbit secondary antibodies conjugated to Alexa Fluor 405, 488, 555, or 647 (Invitrogen). Anti–α-tubulin was used at 1:500, anti–acetylated tubulin was used at 1:200, and all secondary antibodies were used at 1:300.

Confocal microscopy

Imaging of live/fixed cells was performed with an inverted fluorescence microscope (TE2000-U; Nikon) equipped with an electron-multiplying charge-coupled device camera (Cascade II; Photometrics) and a Yokogawa spinning disc confocal system (CSU-Xm2; Nikon). Images were taken with a 100× NA 1.4 oil objective, and live imaging was performed at 37°C. Images were acquired using MetaMorph (version 7.0; MDS Analytical Technologies) and contrasted and merged using Photoshop (Adobe) or MetaMorph. Scale bars were generated using either MetaMorph or ImageJ (National Institutes of Health).

MT curvature analysis

The length of MTs to be analyzed for curvature was measured using MetaMorph, and images of MTs were cropped to the appropriate size. For measuring the curvature of acetylated and nonacetylated MTs, this length was a total of 5 µm. For measuring ER sliding events, EB3-labeled dynamic MTs, and MTs involved in TAC events, this length was a minimum of 2 µm. MT curvature was measured by tracing MTs in these cropped images using IMOD (Kremer et al., 1996), and "imodcurvature" was used to determine the mean curvature of each traced MT.

Western blotting

Whole cell lysates of COS-7 cells were resuspended in Laemmli sample buffer, boiled 5 min, separated by SDS-PAGE, and transferred to a polyvinylidene fluoride membrane. Antibody against acetylated tubulin was used at 1:2,000, and antibody against α-tubulin was used at 1:1,000. HRP-conjugated goat anti–rabbit or goat anti–mouse secondary antibodies were used at 1:3,000. Fluorescence was detected with SuperSignal West Pico Chemiluminescent solution (Thermo Fisher Scientific).

Online supplemental material

Fig. S1 shows entire cells used for retrospective ER sliding. Fig. S2 shows MT tracings used to determine curvature. Fig. S3 shows the effect of TSA treatment on MT acetylation in other cell lines. Fig. S4 shows that contact of the ER and mitochondria is maintained despite ionomycin-induced vesiculation of each. Fig. S5 shows that mitochondria dynamics do not increase after TSA treatment. Video 1 shows ER dynamics. Videos 2 and 3 show ER dynamics before and after nocodazole treatment. Videos 4 and 5 show ER dynamics before and after TSA treatment. Videos 6–8 show ER–mitochondria coupled dynamics. Videos 9 and 10 show ER and mitochondria dynamics after nocodazole treatment. Online supplemental material is available at http://www.jcb.org/cgi/content/full/jcb.200911024/DC1.

We thank R. McIntosh and C. Pearson for helpful suggestions, M. Winey for critical reading of this manuscript, D. Chan, A. English, N. Galjart, T. Meyer, and A. Palmer for expression constructs, and R. Mazitschek and S. Schreiber for the tubacin structural analogue MAZ1370 (with funding from the National Cancer Institute's Initiative for Chemical Genetics, contract number N01-CO-12400).

J.R. Friedman is supported by National Institutes of Health (NIH) training grant GM08759. B.M. Webster is supported by a grant from the Undergraduate Research Opportunity Program at the University of Colorado at Boulder. K.J. Verhey is supported by NIH grant GM083254. D.N. Mastronarde is supported by a grant to A.H. Hoenger from the National Center for Research Resources (P41-RR000592). G.K. Voeltz is supported by a Searle Scholar award and by NIH grant GM083977.

Submitted: 4 November 2009
Accepted: 14 July 2010

References

Baumann, O., and B. Walz. 2001. Endoplasmic reticulum of animal cells and its organization into structural and functional domains. *Int. Rev. Cytol.* 205:149–214. doi:10.1016/S0074-7696(01)05004-5

Bicek, A.D., E. Tüzel, D.M. Kroll, and D.J. Odde. 2007. Analysis of microtubule curvature. *Methods Cell Biol.* 83:237–268. doi:10.1016/S0091-679X(07)83010-X

Boldogh, I.R., and L.A. Pon. 2007. Mitochondria on the move. *Trends Cell Biol.* 17:502–510. doi:10.1016/j.tcb.2007.07.008

Cai, D., D.P. McEwen, J.R. Martens, E. Meyhofer, and K.J. Verhey. 2009. Single molecule imaging reveals differences in microtubule track selection between Kinesin motors. *PLoS Biol.* 7:e1000216. doi:10.1371/journal.pbio.1000216

Cambray-Deakin, M.A., S.J. Robson, and R.D. Burgoyne. 1988. Colocalisation of acetylated microtubules, glial filaments, and mitochondria in astrocytes in vitro. *Cell Motil. Cytoskeleton*. 10:438–449. doi:10.1002/cm.970100311

Csordás, G., C. Renken, P. Várnai, L. Walter, D. Weaver, K.F. Buttle, T. Balla, C.A. Mannella, and G. Hajnóczky. 2006. Structural and functional features and significance of the physical linkage between ER and mitochondria. *J. Cell Biol.* 174:915–921. doi:10.1083/jcb.200604016

de Brito, O.M., and L. Scorrano. 2008. Mitofusin 2 tethers endoplasmic reticulum to mitochondria. *Nature*. 456:605–610. doi:10.1038/nature07534

Eden, E.R., I.J. White, A. Tsapara, and C.E. Futter. 2010. Membrane contacts between endosomes and ER provide sites for PTP1B-epidermal growth factor receptor interaction. *Nat. Cell Biol.* 12:267–272.

English, A.R., N. Zurek, and G.K. Voeltz. 2009. Peripheral ER structure and function. *Curr. Opin. Cell Biol.* 21:596–602. doi:10.1016/j.ceb.2009.04.004

Frederick, R.L., and J.M. Shaw. 2007. Moving mitochondria: establishing distribution of an essential organelle. *Traffic*. 8:1668–1675. doi:10.1111/j.1600-0854.2007.00644.x

Grigoriev, I., S.M. Gouveia, B. van der Vaart, J. Demmers, J.T. Smyth, S. Honnappa, D. Splinter, M.O. Steinmetz, J.W. Putney Jr., C.C. Hoogenraad, and A. Akhmanova. 2008. STIM1 is a MT-plus-end-tracking protein involved in remodeling of the ER. *Curr. Biol.* 18:177–182. doi:10.1016/j.cub.2007.12.050

Haggarty, S.J., K.M. Koeller, J.C. Wong, C.M. Grozinger, and S.L. Schreiber. 2003. Domain-selective small-molecule inhibitor of histone deacetylase 6 (HDAC6)-mediated tubulin deacetylation. *Proc. Natl. Acad. Sci. USA*. 100:4389–4394. doi:10.1073/pnas.0430973100

Hammond, J.W., C.-F. Huang, S. Kaech, C. Jacobson, G. Banker, and K.J. Verhey. 2010. Posttranslational modifications of tubulin and the polarized transport of kinesin-1 in neurons. *Mol. Biol. Cell*. 21:572–583. doi:10.1091/mbc.E09-01-0044

Hoepfner, S., F. Severin, A. Cabezas, B. Habermann, A. Runge, D. Gillooly, H. Stenmark, and M. Zerial. 2005. Modulation of receptor recycling and degradation by the endosomal kinesin KIF16B. *Cell*. 121:437–450. doi:10.1016/j.cell.2005.02.017

Hom, J.R., J.S. Gewandter, L. Michael, S.S. Sheu, and Y. Yoon. 2007. Thapsigargin induces biphasic fragmentation of mitochondria through calcium-mediated mitochondrial fission and apoptosis. *J. Cell. Physiol.* 212:498–508. doi:10.1002/jcp.21051

Hubbert, C., A. Guardiola, R. Shao, Y. Kawaguchi, A. Ito, A. Nixon, M. Yoshida, X.-F. Wang, and T.-P. Yao. 2002. HDAC6 is a microtubule-associated deacetylase. *Nature*. 417:455–458. doi:10.1038/417455a

Hurd, D.D., and W.M. Saxton. 1996. Kinesin mutations cause motor neuron disease phenotypes by disrupting fast axonal transport in *Drosophila*. *Genetics*. 144:1075–1085.

Koeller, K.M., S.J. Haggarty, B.D. Perkins, I. Leykin, J.C. Wong, M.-C.J. Kao, and S.L. Schreiber. 2003. Chemical genetic modifier screens: small molecule trichostatin suppressors as probes of intracellular histone and tubulin acetylation. *Chem. Biol.* 10:397–410. doi:10.1016/S1074-5521(03)00093-0

Kornmann, B., E. Currie, S.R. Collins, M. Schuldiner, J. Nunnari, J.S. Weissman, and P. Walter. 2009. An ER-mitochondria tethering complex revealed by a synthetic biology screen. *Science*. 325:477–481. doi:10.1126/science.1175088

Kremer, J.R., D.N. Mastronarde, and J.R. McIntosh. 1996. Computer visualization of three-dimensional image data using IMOD. *J. Struct. Biol.* 116:71–76. doi:10.1006/jsbi.1996.0013

Lee, C., and L.B. Chen. 1988. Dynamic behavior of endoplasmic reticulum in living cells. *Cell*. 54:37–46. doi:10.1016/0092-8674(88)90177-8

Levine, T., and C. Loewen. 2006. Inter-organelle membrane contact sites: through a glass, darkly. *Curr. Opin. Cell Biol.* 18:371–378. doi:10.1016/j.ceb.2006.06.011

Liou, J., M.L. Kim, W.D. Heo, J.T. Jones, J.W. Myers, J.E. Ferrell Jr., and T. Meyer. 2005. STIM is a Ca2+ sensor essential for Ca2+-store-depletion-triggered Ca2+ influx. *Curr. Biol.* 15:1235–1241. doi:10.1016/j.cub.2005.05.055

Liou, J., M. Fivaz, T. Inoue, and T. Meyer. 2007. Live-cell imaging reveals sequential oligomerization and local plasma membrane targeting of stromal interaction molecule 1 after Ca2+ store depletion. *Proc. Natl. Acad. Sci. USA*. 104:9301–9306. doi:10.1073/pnas.0702866104

Loktev, A.V., Q. Zhang, J.S. Beck, C.C. Searby, T.E. Scheetz, J.F. Bazan, D.C. Slusarski, V.C. Sheffield, P.K. Jackson, and M.V. Nachury. 2008. A BBSome subunit links ciliogenesis, microtubule stability, and acetylation. *Dev. Cell*. 15:854–865. doi:10.1016/j.devcel.2008.11.001

Perktold, A., B. Zechmann, G. Daum, and G. Zellnig. 2007. Organelle association visualized by three-dimensional ultrastructural imaging of the yeast cell. *FEMS Yeast Res.* 7:629–638. doi:10.1111/j.1567-1364.2007.00226.x

Piperno, G., M. LeDizet, and X.J. Chang. 1987. Microtubules containing acetylated alpha-tubulin in mammalian cells in culture. *J. Cell Biol.* 104:289–302. doi:10.1083/jcb.104.2.289

Reed, N.A., D. Cai, T.L. Blasius, G.T. Jih, E. Meyhofer, J. Gaertig, and K.J. Verhey. 2006. Microtubule acetylation promotes kinesin-1 binding and transport. *Curr. Biol.* 16:2166–2172. doi:10.1016/j.cub.2006.09.014

Rink, J., E. Ghigo, Y. Kalaidzidis, and M. Zerial. 2005. Rab conversion as a mechanism of progression from early to late endosomes. *Cell*. 122:735–749. doi:10.1016/j.cell.2005.06.043

Rizzuto, R., P. Pinton, W. Carrington, F.S. Fay, K.E. Fogarty, L.M. Lifshitz, R.A. Tuft, and T. Pozzan. 1998. Close contacts with the endoplasmic reticulum as determinants of mitochondrial Ca2+ responses. *Science*. 280:1763–1766. doi:10.1126/science.280.5370.1763

Rocha, N., C. Kuijl, R. van der Kant, L. Janssen, D. Houben, H. Janssen, W. Zwart, and J. Neefjes. 2009. Cholesterol sensor ORP1L contacts the ER protein VAP to control Rab7–RILP–p150^{Glued} and late endosome positioning. *J. Cell Biol.* 185:1209–1225. doi:10.1083/jcb.200811005

Song, Z., M. Ghochani, J.M. McCaffery, T.G. Frey, and D.C. Chan. 2009. Mitofusins and OPA1 mediate sequential steps in mitochondrial membrane fusion. *Mol. Biol. Cell*. 20:3525–3532. doi:10.1091/mbc.E09-03-0252

Staehelin, L.A. 1997. The plant ER: a dynamic organelle composed of a large number of discrete functional domains. *Plant J.* 11:1151–1165. doi:10.1046/j.1365-313X.1997.11061151.x

Stepanova, T., J. Slemmer, C.C. Hoogenraad, G. Lansbergen, B. Dortland, C.I. De Zeeuw, F. Grosveld, G. van Cappellen, A. Akhmanova, and N. Galjart. 2003. Visualization of microtubule growth in cultured neurons via the use of EB3-GFP (end-binding protein 3-green fluorescent protein). *J. Neurosci.* 23:2655–2664.

Subramanian, K., and T. Meyer. 1997. Calcium-induced restructuring of nuclear envelope and endoplasmic reticulum calcium stores. *Cell*. 89:963–971. doi:10.1016/S0092-8674(00)80281-0

Tanaka, Y., Y. Kanai, Y. Okada, S. Nonaka, S. Takeda, A. Harada, and N. Hirokawa. 1998. Targeted disruption of mouse conventional kinesin heavy chain, kif5B, results in abnormal perinuclear clustering of mitochondria. *Cell*. 93:1147–1158. doi:10.1016/S0092-8674(00)81459-2

Terasaki, M., L.B. Chen, and K. Fujiwara. 1986. Microtubules and the endoplasmic reticulum are highly interdependent structures. *J. Cell Biol.* 103:1557–1568. doi:10.1083/jcb.103.4.1557

Vance, J.E. 2008. Phosphatidylserine and phosphatidylethanolamine in mammalian cells: two metabolically related aminophospholipids. *J. Lipid Res.* 49:1377–1387. doi:10.1194/jlr.R700020-JLR200

Vedrenne, C., and H.-P. Hauri. 2006. Morphogenesis of the endoplasmic reticulum: beyond active membrane expansion. *Traffic*. 7:639–646. doi:10.1111/j.1600-0854.2006.00419.x

Voeltz, G.K., W.A. Prinz, Y. Shibata, J.M. Rist, and T.A. Rapoport. 2006. A class of membrane proteins shaping the tubular endoplasmic reticulum. *Cell*. 124:573–586. doi:10.1016/j.cell.2005.11.047

Waterman-Storer, C.M., and E.D. Salmon. 1998. Endoplasmic reticulum membrane tubules are distributed by microtubules in living cells using three distinct mechanisms. *Curr. Biol.* 8:798–806. doi:10.1016/S0960-9822(98)70321-5

Woźniak, M.J., B. Bola, K. Brownhill, Y.-C. Yang, V. Levakova, and V.J. Allan. 2009. Role of kinesin-1 and cytoplasmic dynein in endoplasmic reticulum movement in VERO cells. *J. Cell Sci.* 122:1979–1989. doi:10.1242/jcs.041962